2007-12-01

A Coupled Fluid-structure Model of a Therapeutic Ultrasound Angioplasty Wire Waveguide

Graham Gavin
Technological University Dublin, graham.gavin@tudublin.ie

Finbar Dolan
Medtronic Vascular Ltd, Galway

M.S. Hashmi
Dublin City University

Garrett McGuinness
Dublin City University

Recommended Citation

Gavin, G., Dolan, F., Hashmi, M., McGuinness G.: A Coupled Fluid-Structure Model of a Therapeutic Ultrasound Angioplasty Wire Waveguide. Journal of Medical Devices, Vol. 1, , pp 254-263. December, 2007. doi:10.21427/7ag6-ex70

A Coupled Fluid-Structure Model of a Therapeutic Ultrasound Angioplasty Wire Waveguide

Graham P. Gavin*, Finbar Dolan**, M.S.J. Hashmi** and Garrett B. McGuinness**

* School of Manufacturing and Design Engineering, Dublin Institute of Technology, Dublin, Ireland

** School of Mechanical and Manufacturing Engineering, Dublin City University, Ireland

*** Medtronic Vascular Ltd., Galway, Ireland

Abstract

Ultrasonic longitudinal displacements, delivered to the distal tips of small diameter wire waveguides, have been shown to be capable of disrupting complicated atherosclerotic plaques during vascular interventions. These ultrasonic displacements can disrupt plaques by direct contact ablation but also by pressure waves, associated cavitation and acoustic streaming developed in the surrounding blood and tissue cavities. The pressure waves developed within the arterial lumen appear to play a major role but are complex to predict as they are determined by the distal tip output of the wire waveguide (both displacement and frequency), the geometric features of the waveguide tip and the effects of biological fluid interactions. This work describes a numerical linear acoustic fluid-structure model of an ultrasonic wire waveguide and the blood surrounding the distal-tip. The model predicts a standing wave structure in the wire waveguide, including the stresses and the displacements, with the inclusion of a validated damping constant. The effects of including an enlarged ball-tip at the distal end of the waveguide, designed to enhance cavitation and surface contact area, are investigated, in addition to the effects of the surrounding blood on the resonant response of the waveguide. The model predicts the pressures developed in the acoustic fluid field surrounding the ultrasonic vibrating waveguide tip and can predict the combinations of displacements, frequencies and waveguide geometries required to cause cavitation, an important event in the disruption of plaque. The model has been validated against experimental displacement measurements with a purpose built 23.5 kHz nickel titanium wire waveguide apparatus and against experimental pressure measurements from the literature.

Nomenclature

u	*harmonic displacement amplitude at any point in a uniform rod*
x	*the distance from the proximal end of uniform rod*
t	*time*
l	*length of a uniform rod*
b	*input displacement amplitude*
ω	*angular frequency*
c	*longitudinal speed of sound in a medium*
f	*frequency (Hz)*
P	*Pressure Amplitude*
ρ	*density*
d	*displacement amplitude*
R	*radius of sphere*
r	*radial location in a field*
θ	*angular location in a field*
E	*Young's Modulus*
$[K]$	*stiffness matrix*
$[M]$	*mass matrix*
$(\ddot{\vec{u}})$	*nodal acceleration vector*
$(\dot{\vec{u}})$	*nodal velocity vector*
$(\vec{u})$	*nodal displacement vector*
$(\vec{F}^{a})$	*applied load vector*
$[C]$	*damping matrix*
$(\ddot{\vec{P}})$	*2nd derivative of nodal pressure*
$(\vec{P})$	*nodal pressure*
$[R]$	*coupling matrix*

Note: All displacements used are peak-to-peak displacements unless otherwise stated

1. Introduction

The majority of coronary atherosclerotic plaques are currently treated by minimally invasive dilation procedures, such as balloon angioplasty and stent implantation, which achieve their goal, primarily, by the mechanical loading and disruption of the plaque material. Annually, approximately two million interventions are carried out in the United States at an estimated annual cost to the economy of $393.5 billion [1]. These procedures rely on a guidewire gaining prior access to and crossing the diseased tissue, acting as a guide rail for the dilation catheter [2 and 3]. Complications occur when the arterial lumen is near or totally occluded and the guidewire cannot cross the lesion, preventing the application of these standard procedures. These plaques are known as chronic total occlusions (CTOs) and may represent up to 16 % of all coronary plaques [2].

The use of high-amplitude (0-150 μm) low-frequency ultrasound (0- 45 kHz) delivered to the distal-tip of small diameter wire waveguides has been shown to disrupt calcified and fibrous plaque material *in vivo* [4, 5 and 6]. Currently (2006), clinical trials are underway in the United States to assess the safety and effectiveness of this form of technology as a novel means of crossing CTOs with very promising initial reports [7, 8 and 9]. These devices operate by generating the ultrasonic displacements external to the body by means of an ultrasonic generator and piezoelectric converter with a fixed operating resonant frequency, as shown in Figure 1. These displacements are further amplified by means of a tapered acoustic horn that is also designed to resonate at the frequency of the converter [10].

A small diameter wire waveguide, often made from an alloy of titanium or aluminium, is mechanically coupled to the radiating face of the acoustic horn. This method allows for minimal invasive delivery of the ultrasonic displacements, via the wire waveguide, through the tortuous vascular structure to the lesion location [5 and 6]. Atar *et al* [11] suggested that plaque disruption was due to direct contact ablation between the wire waveguide distal tip and the plaque and also, due to cavitation, pressure waves and acoustic streaming developed in the surrounding fluid. Cavitation appears to play a major role and some authors have concluded that ultrasound ablation *in vitro* was only evident above the cavitation threshold [12].

The majority of work in the literature has been focused on the end clinical results during *in vitro* and *in vivo* studies with less detailed investigation into the mechanical effects of this form of ultrasound in small diameter waveguides and on surrounding biological fluid. Some authors, however, have performed experimental studies to further understand potential biomechanical disruptive events due to the ultrasonic vibrating wire waveguide distal tip. Makin and Everbach [13] performed experimental pressure measurements in fluid (glycerine/water blood model fluid) surrounding the distal-tip of a 22.5 kHz ultrasonic wire waveguide device. The device delivered ultrasonic displacements down waveguides of lengths of up to 660 mm, with enlarged ball-tips located at the distal-end. The use of a ball-tip at the distal end of wire waveguides has been reported by many authors in clinical studies and is used to increase the area of the waveguide in contact with the lesion and surrounding fluid, increasing acoustic pressures and enhancing the possibility of cavitation [14]. The results from Makin and Everbach's experiments show the pressure field in the region (12 mm – 200 mm) surrounding the vibrating waveguide and the authors suggested that the acoustic pressures near

the distal-tip would be of sufficient amplitude to generate the cavitation that was observed. Experimental measurements within 12 mm of the tip were not obtained due to experimental limitations.

The effect of wire length on the peak to peak displacement output of a wire waveguide has been previously investigated by the present authors and a finite element model capable of predicting the distal tip response of wire waveguides, to periodic sinusoidal inputs, in the ultrasonic range has also been developed and validated with the inclusion of an appropriate damping value [15 and 16]. This model, however, does not account for the effect of acoustic fluid-structure interactions at the waveguide tip, and does not therefore model the effect of acoustic forces on the wire waveguide or predict the acoustic pressure field generated in surrounding blood by the ultrasonic waveguide tip. A complete model incorporating these effects is a necessary tool for the design and optimisation of flexible ultrasonic waveguides for minimally invasive procedures and also in further understanding *in vivo* conditions during ultrasonic angioplasty procedures.

Of interest, also, are the effects of having an enlarged distal tip in the presence of fluid, on the waveguide resonant response and on the pressure field developed around the vibrating distal tip. While analytical solutions applicable to both the waveguide and the fluid response are reported in the literature and are discussed as part of this work, they are limited to simple uniform geometries and conditions. The use of the finite element method will prove beneficial in determining wire waveguide behaviour and the acoustic pressures in the region close to the distal-tip, for a range of frequencies, displacements and in predicting the effects of more complex geometry and conditions, associated with *in vivo* application.

The aim of this research is to develop an acoustic fluid-structure linear numerical model of an ultrasonic wire waveguide and the fluid surrounding the distal-tip. It will be used to predict the steady-state harmonic waveguide response to a prescribed input displacement at the proximal end and to predict displacements and stresses along the total length of the waveguide. The effects of including an enlarged distal-tip and the presence of a fluid on the resonant response of the waveguide are also investigated. The inclusion of the fluid, coupled to the distal-tip of the wire waveguide, will allow for the prediction of pressures developed in the fluid field and will be used to help predict when highly disruptive cavitation may occur.

2. Materials and Methods

A. Description of the Experimental Apparatus

The purpose built ultrasonic wire waveguide apparatus used in the experimental displacement measurements is similar to devices reported elsewhere and in clinical trials [7 and 13]. It consists of a piezoelectric converter and titanium acoustic horn, adapted from sonochemistry applications (Branson Ultrasonics, Danbury, CT) and is described in more detail elsewhere [15 and 16]. It has an operational frequency of 23.5 kHz and delivers longitudinal displacements of up to 100 µm peak-to-peak to the proximal end of 1.0 mm diameter nickel-titanium (NiTi, Fort Wayne Metals, Fort Wayne, IN) wire waveguides. The ultrasonic generator can allow the input displacement delivered to the proximal (input) end of the waveguide to be controlled. The NiTi wire waveguides used were uniform in diameter and have no enlarged distal-tip geometry.

B. Optical Displacement Measurement

The wire waveguide displacements were measured by optical measurement techniques. This involved the direct measurement of the peak-to-peak displacements, observed as streaks, using an optical microscope (SPS Laboratories), a digital colour camera (Vantage 'VGC400') and a PC with calibrated image analysis software (Image Analysis System, Buehler). This method was reported previously by the present authors and in the literature [10 and 15] in measuring the waveguide distal tip displacements and the results from those studies are shown in Figures 2a and 2b.

Expanding on this previous work, displacements at any point along the length of the waveguide were measured in a similar manner, by focussing on a mark on the waveguide's oxidized surface and by capturing and measuring the displacement during ultrasonic activation. These measurements were made for a waveguide with an input displacement of 32 µm (10 Watts (RMS)) and multiple wire waveguide lengths. Figure 3 shows an image of a vibrating point on the waveguide captured using the optical method. Measurements at lengths less than 118 mm could not be achieved due to the physical constraints of the microscope and the apparatus. At wire waveguide lengths close to resonant lengths measurements could not be made as it is a characteristic of the ultrasonic apparatus not to deliver power in this region.

C. Characteristics of Wire Waveguide

The steady-state analytical solution of motion for an undamped longitudinally vibrating rod, as shown in Figure 4, subjected to a sinusoidal input vibration motion of $u(t) = b \sin\omega t$, is given in Equation 1 [17]. This can be used to represent ultrasound transmitted via a wire waveguide, where the distal-tip of the acoustic horn applies a sinusoidal input of prescribed amplitude and frequency to the proximal end of the wire waveguide.

$$u(x,t) = b(\cos\frac{\omega x}{c} + \tan\frac{\omega l}{c}\sin\frac{\omega x}{c})\sin\omega t \qquad (1)$$

This analytical solution assumes that there is no damping in the uniform rod and that the distal end is in a stress free state (unloaded). In the ultrasound angioplasty application, damping is present in the wire waveguide due to internal friction in the waveguide material and there is also loading on the distal-end of the waveguide due to presence of an enlarged distal-tip (lumped mass) and the surrounding fluid. The material and acoustic properties of the NiTi wire, used in the waveguide, were obtained from the manufacturer and are presented in Table 1.

D. Characteristics of Spherical Acoustic Source

An analytical solution exists for the pressure field developed in the fluid surrounding an oscillating sphere, as shown in Equation 2 and Figure 5 [14 and 18]. In this solution the pressure amplitude, P_{max}, at any point in the field, surrounding an oscillating sphere, can be determined as follows.

$$P_{\max} = 2\pi^2 \rho R f^2 d_0 \times \frac{R^2 |\cos\theta|}{r^2} \tag{2}$$

This solution shows that the pressure amplitudes are at a maximum on the surface of the sphere and directly ahead of it. The solution is limited to a simple spherical ball in a fluid. Knowledge of the pressures developed is crucial, as in the frequency range used in ultrasound angioplasty the pressure at which cavitation will take place lies in the range between 100- 300 kPa [10 and 14], depending of the amount dissolved gasses in the fluid or introduced by the device. Cavitation around the distal-tip may also be further effected by the result of the high velocity fluid flow (acoustic streaming) at the wire tip [13] but are not considered in the analytical or numerical models. The acoustic properties of the blood are presented in Table 1.

E. Numerical Model of Wire Waveguide and Fluid

A 2D axisymmetric finite element model of the wire waveguide and surrounding fluid was developed based on the problem sketch shown in Figure 2. The model was developed in ANSYS© and consists of solid structural elements (Plane42) for the wire waveguide and acoustic fluid elements for the blood (Fluid29). A fluid-structure interface (FSI) is placed at the shared nodes of the fluid and structural element types and an infinite acoustic boundary layer (Fluid129) is located at the extremities of the model preventing acoustic pressure wave reflection. The material properties used for the NiTi wire waveguide and blood are those presented in Table 1.

Figure 6 shows the distal end of the model of a wire waveguide with a spherical distal ball-tip. This is an axisymmetric harmonic model where the steady-state waveguide response to a prescribed longitudinal input displacement is modelled over a set frequency range. The governing equations for both the fluid and structural nodes are shown in Equation 3 and 4, respectively [19].

$$[M_S](\ddot{\vec{u}}) + [C](\dot{\vec{u}}) + [K_S](\vec{u}) = (\vec{F}_S) + [R](\vec{P}) \quad (3)$$

$$[M_F](\ddot{\vec{P}}) + [K_F](\vec{P}) = (\vec{F}_F) - \rho_0 [R]^T (\ddot{\vec{u}}) \quad (4)$$

The damping matrix, [C], in the structural governing equation allows for the inclusion of a constant damping parameter to account for all damping in the waveguide and will be determined by comparing the predicted waveguide response with the experimental displacement measurement results. The wire waveguide configurations modelled were:

a) A wire waveguide (1.0 mm diameter and lengths between 118 - 303 mm) with no distal spherical ball-tip and no fluid present. This is a model of the experimental displacement measurement tests conducted on the purpose built 23.5 kHz apparatus. The displacement results from this model will be compared with the experimental displacement measurements and are used to validate the structural model and further validate the previously determined damping value for the NiTi waveguide at 23.5 kHz [15].

b) Expanding on the model in 'part a)', a wire waveguide (0.35 mm diameter and a length of 500mm) with spherical distal ball-tips of 1.0 mm and 1.5 mm diameters and also, with fluid present. This is more representative of a clinical device's geometry that is described in the literature and in the current clinical trials.

c) A model of the wire waveguide ultrasonic device as described by Makin and Everbach [13]. The experimental pressure measurements made by these authors can be compared with predicted pressure results from the finite element model in the region surrounding the vibrating spherical distal-tip and will be used to validate the fluid results from the model.

3. Results and Discussion

A. Wire Waveguide Structural Results

The analytical solution, shown in Equation 1, predicts a longitudinal standing wave structure in the wire waveguide, with a series of displacement nodes and anti-nodes located at intervals along the length of the waveguide, as determined by the properties (E, ρ) of the waveguide material and frequency of vibration (f). For a wire waveguide of length 288 mm (near an anti-resonant length), the displacement standing wave is shown in Figure 7a for the analytical solution, experimental measurements and numerical model (for two values of damping, equal to 0% (no damping) and 4.5%). The analytical displacement solution predicts a standing wave structure with displacement nodes located at intervals of approximately 75 mm and is closely matched by the predicted numerical displacements with no damping included, as expected. The experimental displacement measurements, also shown in Figure 7a, show a standing wave structure but with notable differences. The standing wave appears to consist of a series of displacement minima and maxima, as opposed to nodes and anti-nodes, and there is also a loss in displacement along the length of the waveguide. With the validated damping value of 4.5 % [15] included, the numerical model shows close agreement with the experimental displacement measurements.

The numerical model also predicts the stresses along the length of the wire waveguide, as shown in the stress plot in Figure 7b, and the importance of damping in correctly predicting the stresses is shown. For the undamped wire waveguide of length 288 mm the predicted stress amplitudes show a series of stress nodes and anti-nodes located at displacement anti-nodes and nodes, respectively. The stress amplitude at the proximal end, a displacement anti-node, is predicted to be 7 MPa. The inclusion of the damping constant greatly affects the predicted stresses along the waveguide. The stress amplitude at the proximal end is now predicted to be 27.3 MPa, with a series of stress minima and maxima along the length of the waveguide. The maximum stress amplitude is located at the first displacement minimum and has a value of 50.5 MPa.

Figure 8a shows the close comparison achieved between the experimental and numerical displacements and also, the predicted stresses (Figure 8b) when the waveguide is operating at a length of 273 mm, approaching a resonant length, and subjected to an applied input displacement of 32 μm. The increased displacements at the distal-tip and along the length of the waveguide are due to the fact that the wire is operating closer to resonance. This increased displacement is accompanied by an overall increase in the predicted stress amplitudes, both at the proximal end and over the length of the waveguide. The stress amplitude at the proximal end of the waveguide is 52.2 MPa and the maximum stress amplitude is 64.7 MPa.

B. Effects of Ball-tip and Fluid (Blood) on Waveguide Resonant Response

The predicted frequency response plot (22- 26 kHz) of the displacement results of a wire waveguide, of length 500 mm and a diameter of 0.35 mm, is shown in Figure 9. The plot includes the frequency response of the waveguide with no distal ball-tip and with spherical distal ball-tips of 1.0 and

1.5 mm diameters over a frequency range of between 20 – 26 kHz. The effect of including a distal ball-tip, similar to a lumped mass, on the waveguide resonant response can be seen. The local anti-resonant frequency of operation of the waveguide shifts from 23.94 kHz to 23.72 kHz for a 1.0 mm tip and to 23.28 kHz for a 1.5 mm tip.

The resonant response results with the distal fluid that surrounds the ball-tip included is shown in Figure 10. The response, both with and without fluid present, for a ball-tip diameter of 1.0 mm is included and for two input proximal displacements of 100 μm and 150 μm. The results show that the presence of the fluid has only a negligible effect on the waveguide frequency response for the ball-tip diameter and the displacements modelled.

C. Acoustic Pressure Results

Figure 11 shows a contour pressure plot of the predicted pressures in the fluid field around a wire waveguide with a 2.46 mm spherical ball-tip, similar to the device described by Makin and Everbach. The results of the predicted pressure amplitudes from the numerical model, in the range of 12 - 100 mm directly ahead of the tip, are shown in Figure 12a and compared with the experimental measurements reported by Makin and Everbach. The predicted pressure results show close comparison with the experimental results for a distal-tip displacement of 130 μm peak-to-peak at a frequency of 22.5 kHz. Figure 12b shows the predicted pressure amplitudes in the region closer to the distal-tip (0-12 mm), where no experimental measurements could obtained. The predicted pressure amplitude at the surface of the ball-tip is 912 kPa. In this region non-linearity's and hydrodynamic effects may play a major role. However, the results show that pressures were of sufficient amplitude to cause the cavitation that was observed by the authors during operation of the device as it is considerably greater than the approximated 200 kPa required to cause cavitation.

Figure 13 shows the predicted acoustic pressures in the fluid field surrounding a 0.35 mm waveguide, with distal ball-tips of 1.0 mm and 1.5 mm diameter and for multiple distal-tip displacements. These dimensions are closer to those required for minimally invasive coronary surgery and described in clinical studies. The results show the effects of increasing the ball-tip diameter on the pressures developed in the surrounding fluid and the approximate displacements required to cause cavitation. With a 1.5 mm ball-tip diameter, the model predicts that a tip displacement of approximately 50 μm peak-to-peak is required to cause cavitation.

Applying this numerical fluid-structure model to the 23.5 kHz in-house ultrasonic wire waveguide apparatus, described as part of this work, the predicted pressure results for multiple distal-tip displacements are shown in Figure 14. These results are for a 1.0 mm diameter wire waveguide with a flat tip and show that a tip displacement of approximately 45-50 μm is required to cause a pressure amplitude of 200 kPa. Figure 15 shows images of the distal-tip of the 23.5 kHz apparatus with a 1.0 mm wire waveguide and for multiple displacements. Based on these experimental observations and the notable change in audible sound when cavitation occurs it was determined that cavitation occurred above a distal-tip displacement of approximately 50-55 μm. This value closely matches the predicted displacement value from the numerical model with the small difference being attributed to dissolved gasses in the water and also introduced gas trapped at the distal-tip of the waveguide acting as nuclei

for cavitation bubbles. Hydrodynamic effects near the waveguide surface, such as acoustic streaming, where fluid velocities are high, may also aid the onset of cavitation at lower tip displacements.

D. Acoustic Streaming

Figure 16 shows an image of the outer acoustic streaming around a 1.0 mm diameter wire waveguide for tip displacements of 35 µm (below cavitation threshold) and 76 µm (above cavitation threshold). These images were captured in water seeded with polyamid particles (Dantec Dynamics 50µm) at ambient temperature. These particles were chosen as they have neutral buoyancy and are commonly used in particle image velocimetry. The images show a unidirectional streaming layer away from the distal-tip which becomes quite violent above the cavitation threshold. While this particular phenomenon is not included in the numerical model these images show the extent of the outer streaming layer while reports in the literature suggest high oscillating velocities and shear stresses in an inner layer [14].

4. Conclusions

The numerical acoustic fluid-structure model of a therapeutic ultrasonic wire waveguide presented can be used to predict, both, the behaviour of the wire waveguide and the pressure in the fluid surrounding the distal tip. The structural displacement results are validated against the experimental displacement measurements made with the 23.5 kHz apparatus and show a standing wave with a series of displacement minima and maxima along the waveguide length. The model shows how the resonant response of the waveguide is affected by the inclusion of an enlarged distal ball tip. The ball tip acts similar to a lumped mass on the distal end of the waveguide and shifts the resonant response. The presence of the fluid around the tip has a negligible effect on the resonant response of the waveguide, in the frequency and displacement range commonly used in clinical applications.

The results for the predicted stresses in the waveguide show the importance of including a correct damping parameter in the model. This results in the stresses at the proximal end of the waveguide being higher than would have been otherwise predicted. These results from the model may further aid in the design of waveguides and reduce failures that are known to occur at the connection point.

The most important benefit of this fluid-structure model of the wire waveguide, appears to be the ability to predict the pressures developed in the fluid field surrounding the distal tip. While the model is a simplified linear acoustic model and has only been validated against results made in the fluid field at a distance of 12 mm from the tip, as reported by Makin and Everbach, its usefulness in predicting the pressures and in understanding the effects of geometry changes, frequency of operation and distal-tip displacements seems apparent. Indeed, in the region close to the vibrating tip, providing conditions are sufficient to cause cavitation, modelling the predicted behaviour may be overly complex due to hydrodynamic effects, non-linear pressure response and the violent cavitation itself.

The model presented as part of this work shows good comparison with both analytical results and experimental measurements and may be a strong starting point in the understanding of waveguide design, the onset of highly disruptive cavitation events and the effects during surgery. The model will prove a valuable design tool in the further development of therapeutic ultrasound wire waveguides as an emerging cardiovascular interventional technique.

Acknowledgements

This work was undertaken in Dublin City University and funded by Enterprise Ireland's Innovation Partnership Agreement in collaboration with Medtronic Vascular, Galway.

References

[1] American Heart Association. Publications, Heart Disease and Stroke Statistics- Update, 2003.

[2] William NG, Wai-Hong Chen, Pui-Yin Lee and Chu-Pak Lau. Initial experience and safety in the treatment of chronic total coronary occlusions with a new optical coherent reflectometry-guided radiofrequency ablation guidewire, *The American Journal of Cardiology*, Volume 92 (6), pp 732-734, 2003.

[3] Harmann A and Kaltenbach M. Chapter 2: Approaches to Total Coronary Occlusions. In: Topol EJ and Serruys PW (eds.). *Current Review of Interventional Cardiology*, Philadelphia, 1994.

[4] Sobbe A, Stumpff U, Trubenstein G, Figge H and Kozuschek W. Die Ultraschall-Auflosung von Thromben. *Klin Wochenschr*, 52, pp 1117- 1121, 1974.

[5] Siegel RJ, Fishbein MC, Forrester J, Moore K, DeCastro E, Daykhovsky Z and Don Michael TA. Ultrasonic Plaque Ablation: a new method for recanalisation of partially or totally occluded arteries. *Circulation*, 78, pp 1443- 1448, 1988.

[6] Rosenschien U, Bernstein J, Di Segni E, Kaplinsky E, Bernheim J and Rozenszain LA. Experimental Ultrasonic angioplasty: disruption of atherosclerotic plaques and thrombi *in vitro* and arterial recanalisation *in vivo*. *J Am Coll Cardiol*., 15, pp 711- 717, 1990.

[7] Melzi G, Colombo A *et al*. Coronay Artery Disease. A novel approach to chronic total occlusions: The crosser system. Catheterization and Cardiovascular Interventions, 2006; 68: 29-35.

[8] Grubbe E *et al*. High frequency mechanical vibration to recanalize chronic total occlusions after failure to cross with conventional guidewires. J Invasive Cardiol, 2006; 18: 85-91.

[9] Joye J. Successful CTO Recanalization. Endovascular Today. 2006; 5 (3): 72-77.

[10] Perkins JP. Power Ultrasonic Equipment: Practice and Application. (Based on a paper presented at the Sonochemistry Symposium. 1986. Annual Chemical Congress, Warwick University, UK, 8-11 April.

[11] Atar S, Luo H, Nagai T, Siegel RJ. Ultrasonic Thrombolysis: catheter-delivered and transcutaneous applications. European Journal of Ultrasound 1999; 9: 39-54.

[12] Yock PG and Fitzgerald PJ. Catheter-based ultrasound thrombolysis: Shake, rattle and reperfuse. Circulation 1997; 95: 1360- 62.

[13] Makin RS and Everbach EC. J. Acoust. Soc. Am. 1996; 100(3): 1855-64.

[14] Nyborg WL. Chapter 1. Basic Physics of Low Frequency Therapuetic Ultrasound. In: Ultrasound Angioplasty. Developments in Cardiovascular Medicine. (Ed. by Siegel RJ). Kluwer Academic Publishers, 1996.

[15] Gavin GP *et al*. Performance characteristics of a therapeutic ultrasound wire waveguide apparatus. International Journal of Mechanical Sciences. 2006; doi: 10.1016/j.ijmecsci.2006.09.006

[16] Gavin GP, GB McGuinness, F Dolan, MSJ Hashmi. 2005. Development and Performance Characteristics of an Ultrasound Angioplasty Device. *Proc. 11th Ann. Conf. BioEng. R. Accad. Med.*, Dublin, Ireland: 78.

[17] Steidel RF (Jr.). 1989. Chapter 13: Distributed Systems. In: An Introduction to Mechanical Vibrations. 3rd Ed, Wiley.

[18] Burdic WS. 1991. Underwater Acoustic System Analysis. 2nd Edition, Prentice Hall.
[19] ANSYS© Help Files. ANSYS© Multiphysics, Version 8.1.

Figures

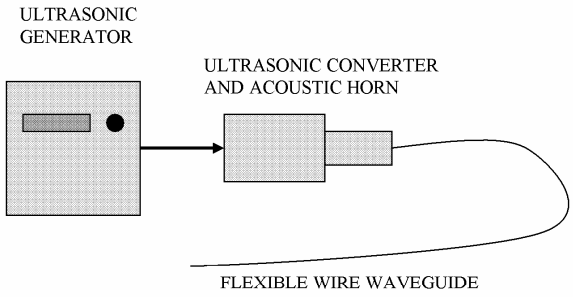

Figure 1: Diagram of therapeutic ultrasound wire waveguide apparatus showing ultrasonic generator, converter and horn, and flexible small diameter wire waveguide

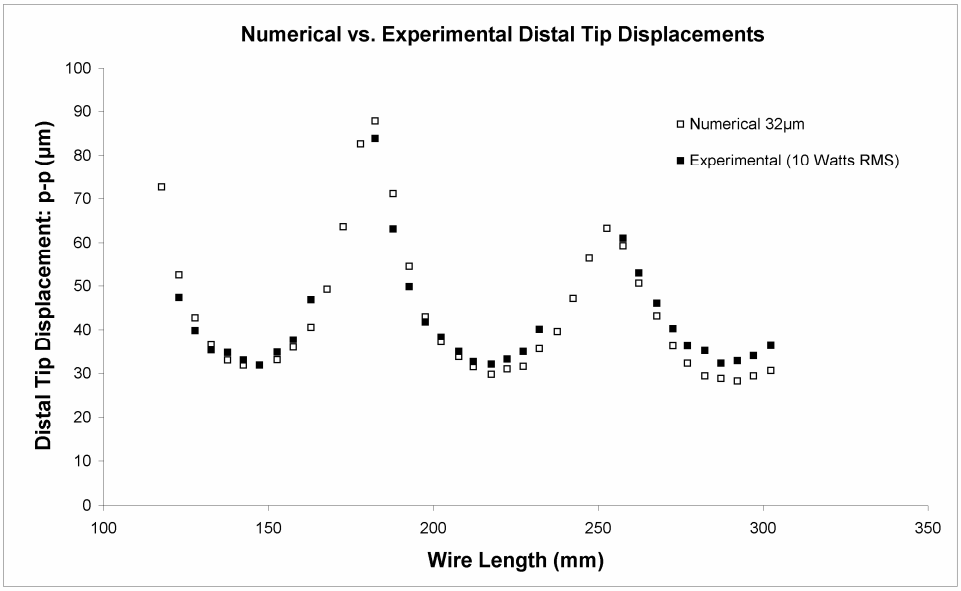

Figure 2a: Comparison of numerical and experimental distal-tip displacements for multiple wire waveguide lengths between 188 mm and 303 mm. Applied proximal displacement is 32 µm. Damping in the waveguide model is 4.5 % [15].

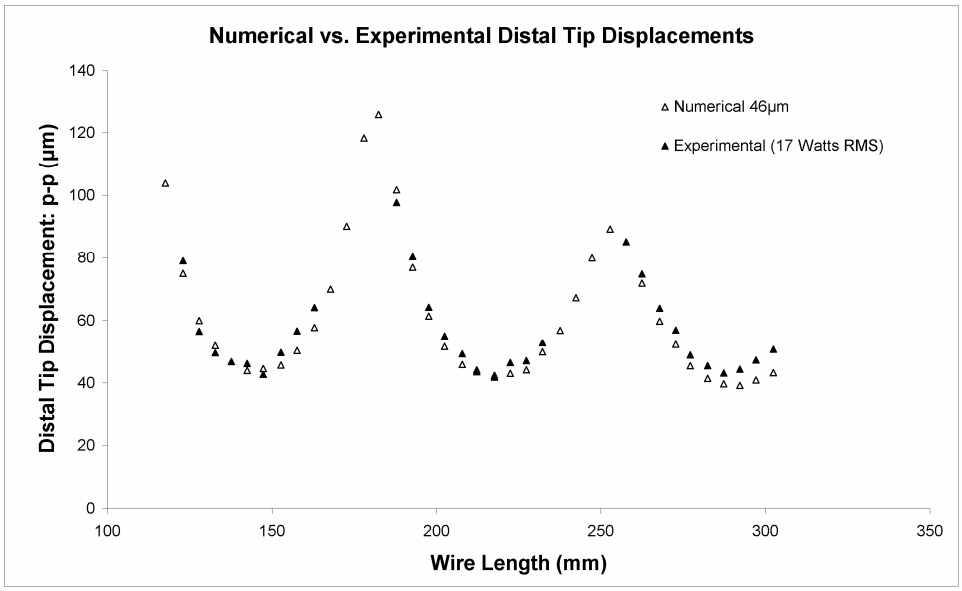

Figure 2b: Comparison of numerical and experimental distal-tip displacements for multiple wire waveguide lengths between 188 mm and 303 mm. Applied proximal displacement is 46 µm. Damping in the waveguide model is 4.5 % [15].

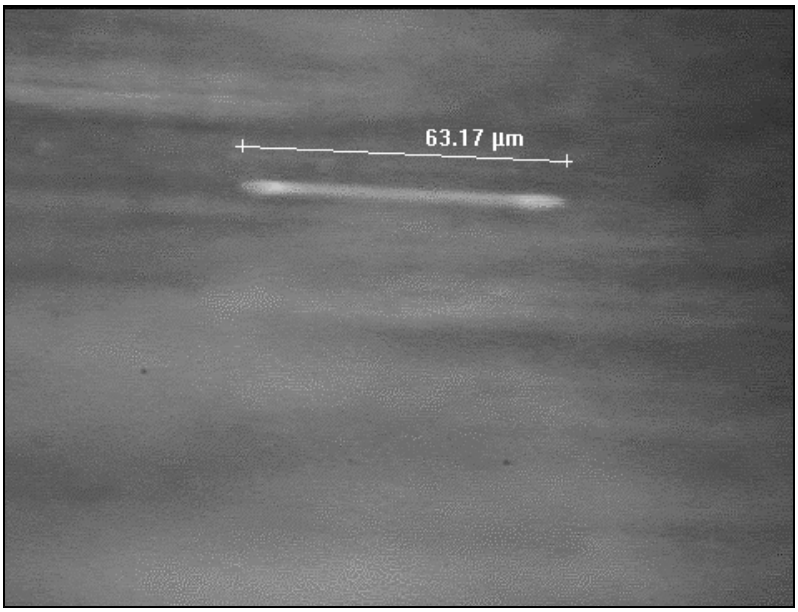

Figure 3: Image of wire waveguide displacement obtained by the optical microscope and image analysis software. Initial length of mark was 9.2µm and the image streak length of 63.17µm giving a displacement of approximately 54 µm peak-to-peak.

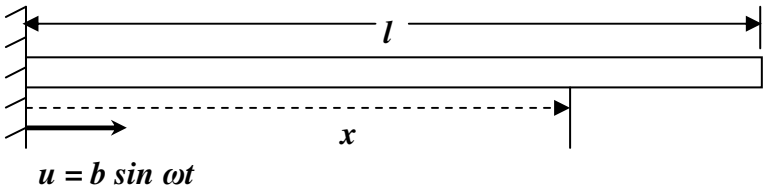

Figure 4: Diagram of a uniform rod, of length *l*, with an input displacement motion of *u = b sin ωt*. Adapted from Steidel [17]

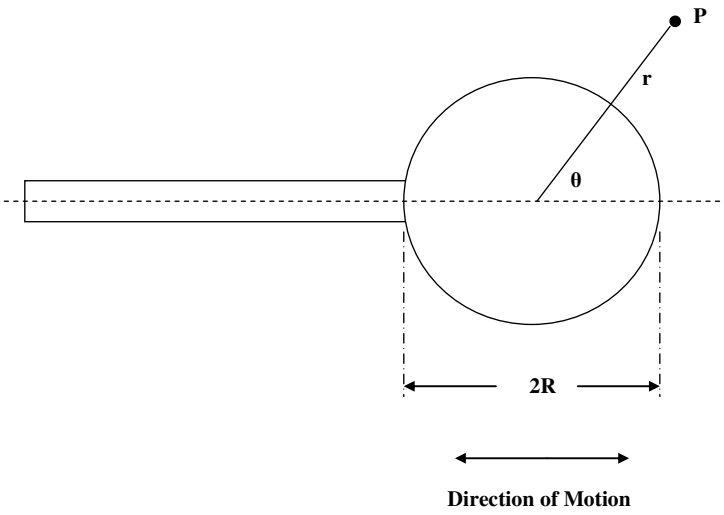

Figure 5: Diagram relating to the pressure field developed around an oscillating sphere. Adapted from Nyborg [14]

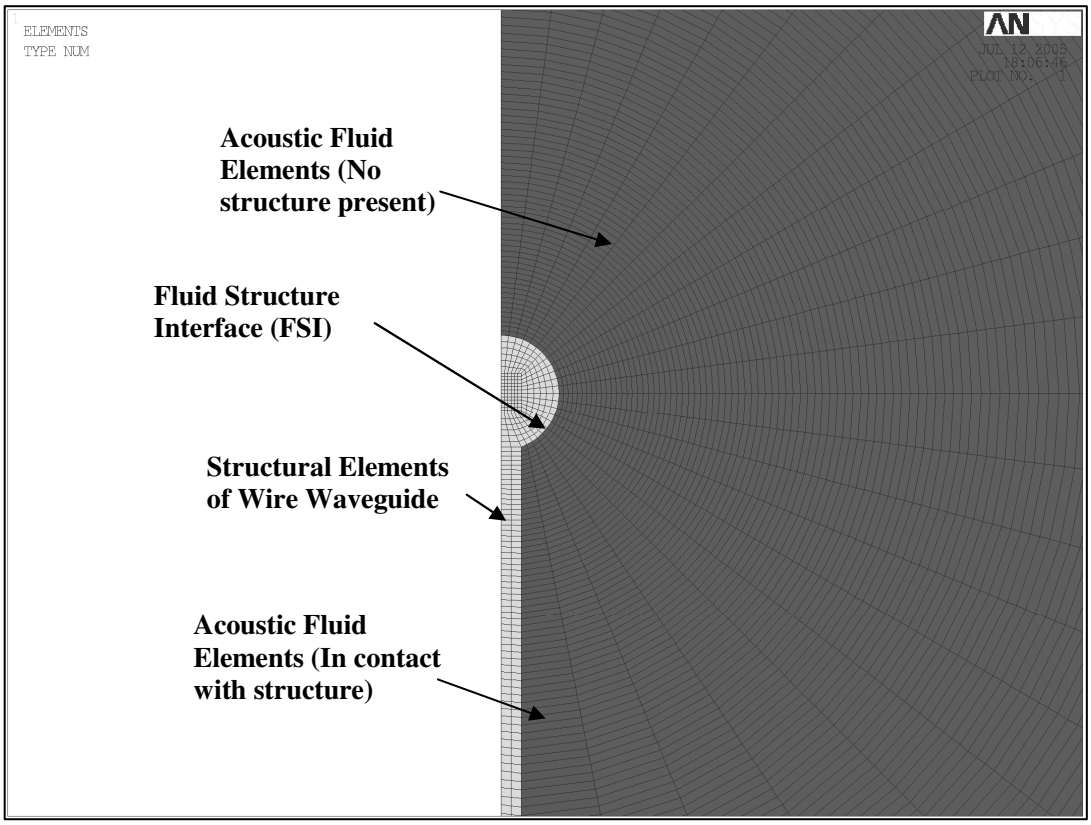

Figure 6: Distal Section of Acoustic Fluid Structure Model of Wire Waveguide with 1.0 mm spherical ball-tip

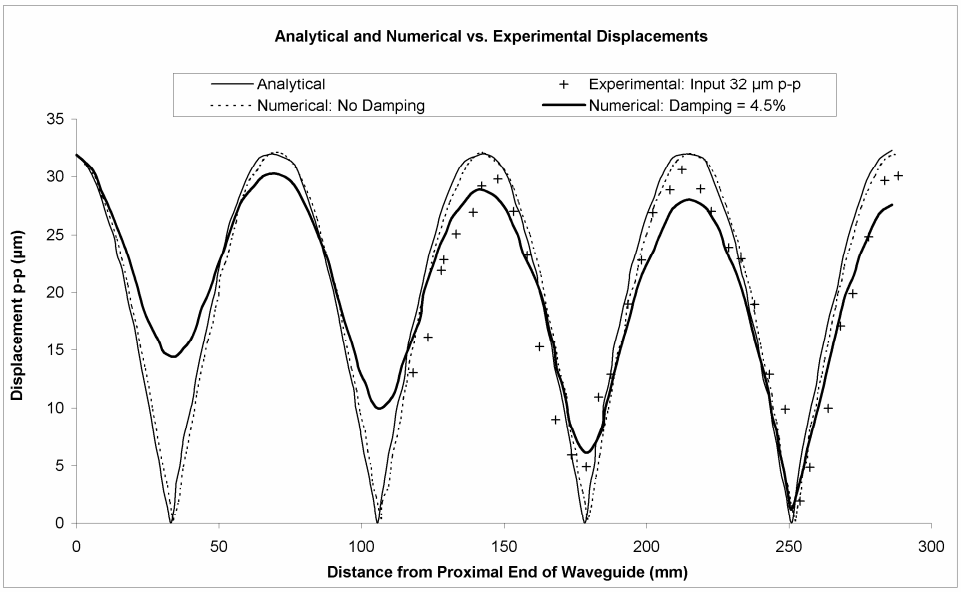

Figure 7a: Comparison of numerical, experimental and analytical displacements for a wire waveguide of length 288 mm (near anti-resonant), with no damping and with 4.5 % damping. Applied proximal displacement is 32 µm.

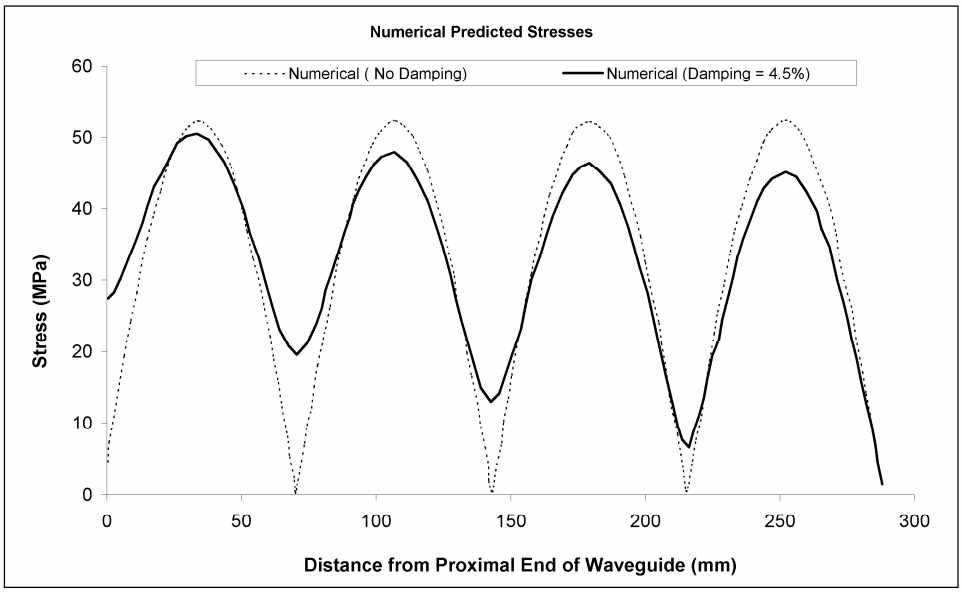

Figure 7b: Comparison of numerical predicted stresses for a wire waveguide of length 288 mm (near anti-resonant), with no damping and with 4.5 % damping. Applied proximal displacement is 32 µm.

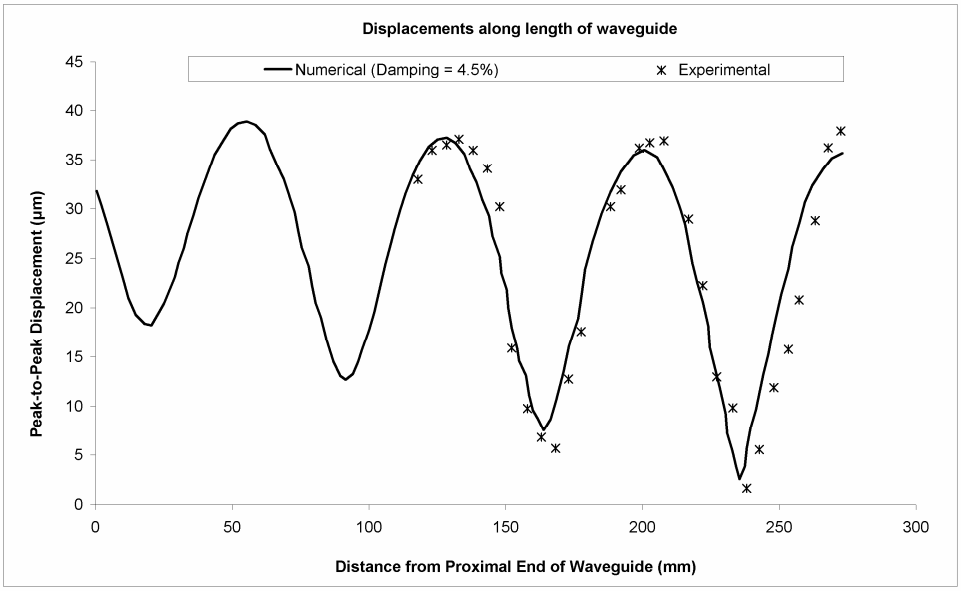

Figure 8a: Comparison of numerical and experimental displacements for a wire waveguide of length 273 mm (near anti-resonant) with 4.5 % damping. Applied proximal displacement is 32 µm.

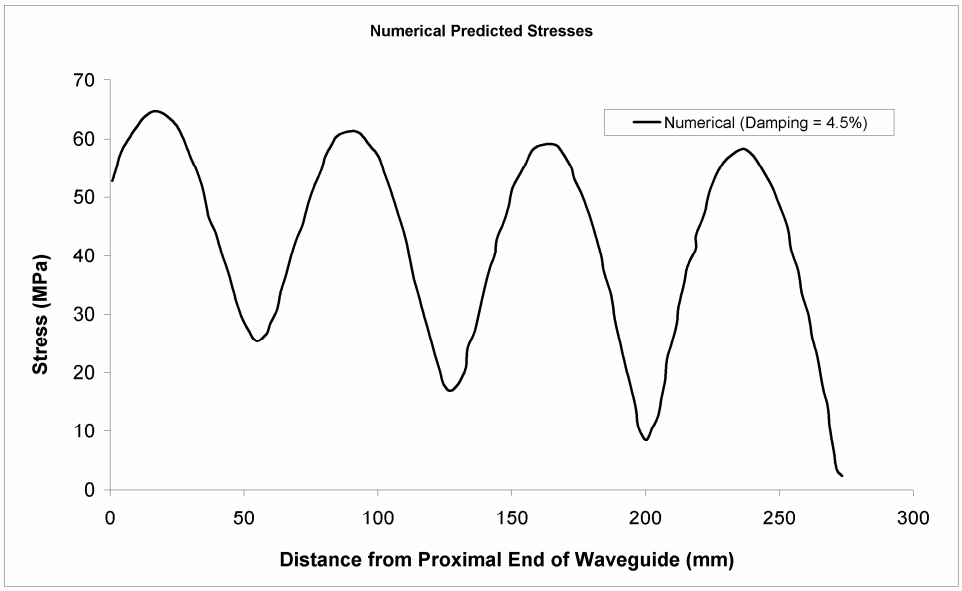

Figure 8b: Numerical predicted stresses for a wire waveguide of length 273 mm (near anti-resonant) with 4.5 % damping. Applied proximal displacement is 32 µm.

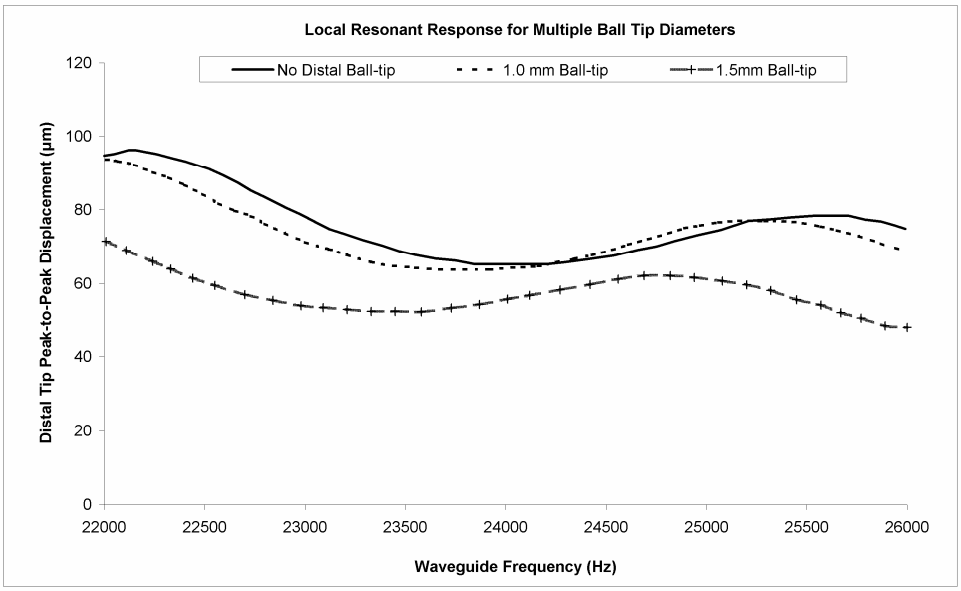

Figure 9: Predicted numerical displacements response for a wire waveguide of length 500 mm and 0.35 mm diameter between 22 - 26 kHz, with no distal ball-tip and ball-tips of 1.0 mm and 1.5 mm. Input displacement is 100 µm. Damping is 4.5 %.

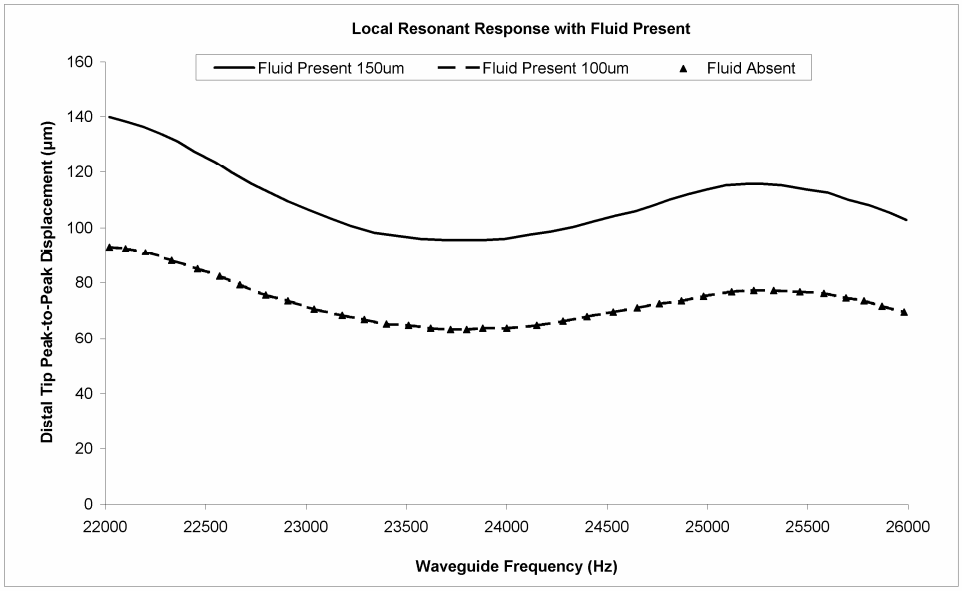

Figure 10: Predicted numerical displacements response for a wire waveguide of length 500 mm and 0.35 mm diameter between 22 - 26 kHz with a 1.0 mm ball-tip. Damping is 4.5%.

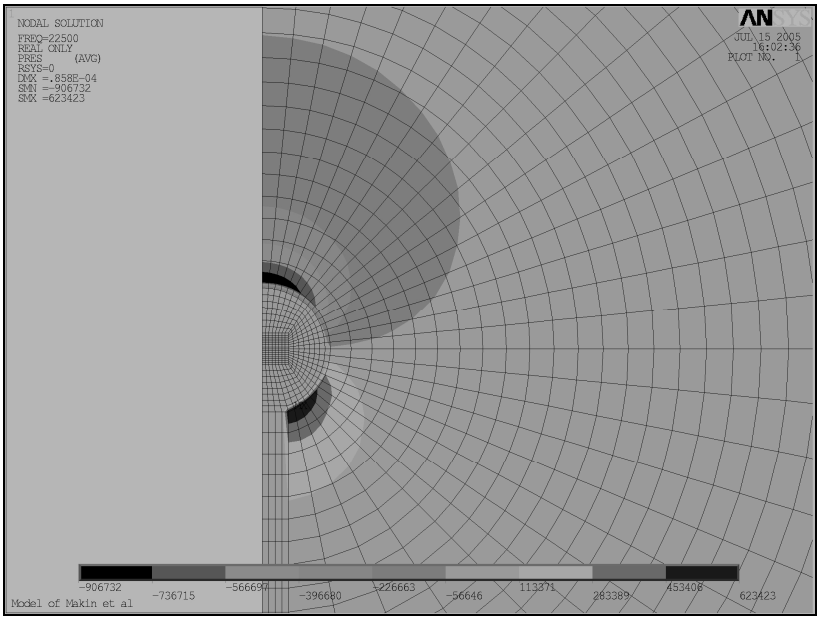

Figure 11: Predicted pressure field around distal section of acoustic fluid structure model of wire waveguide with 2.46 mm spherical ball-tip and distal -tip displacement of 130 μm peak-to-peak at 22.5 kHz. Model based on device described by Makin and Everbach [13]

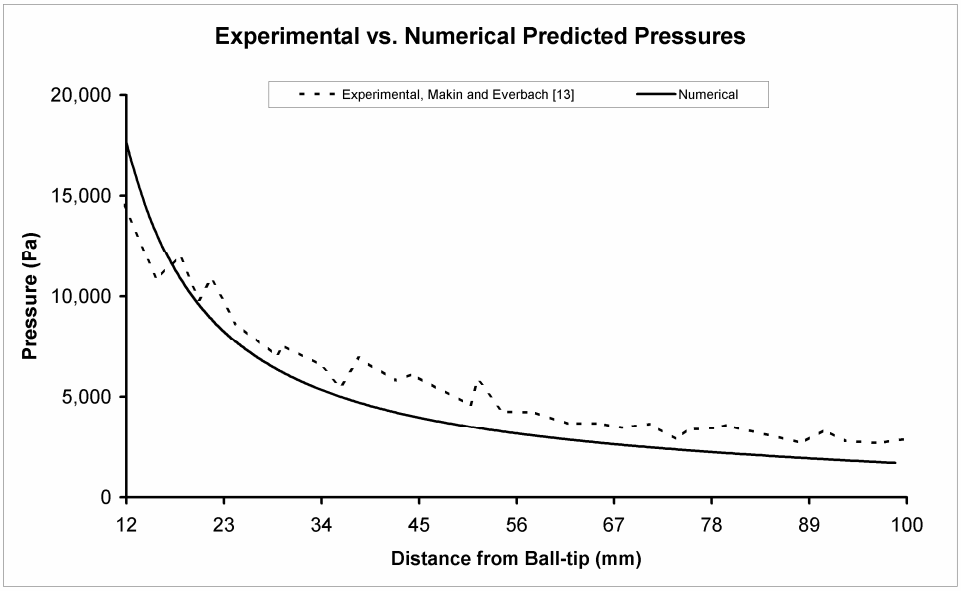

Figure 12a: Experimental pressures and predicted numerical pressure field ahead of 2.46 mm spherical ball-tip, in the region 12 mm -100 mm, and distal -tip displacement of 130 μm at 22.5 kHz. Model based on device described by Makin and Everbach [13]

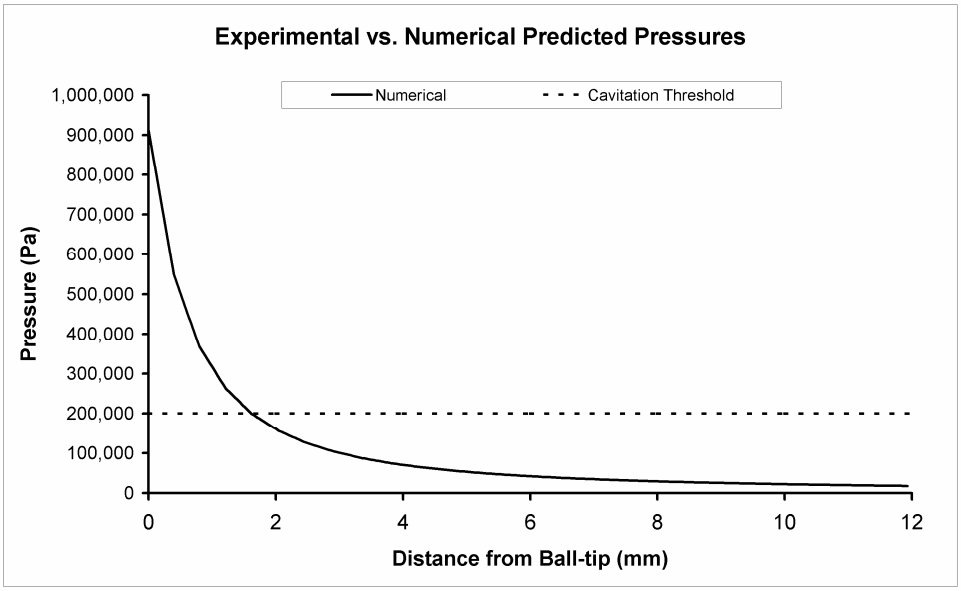

Figure 12b: Experimental pressures and predicted numerical pressure field ahead of 2.46 mm spherical ball-tip, in the region 0 mm -12 mm, and distal -tip displacement of 130 µm at 22.5 kHz. Model based on device described by Makin and Everbach [13]

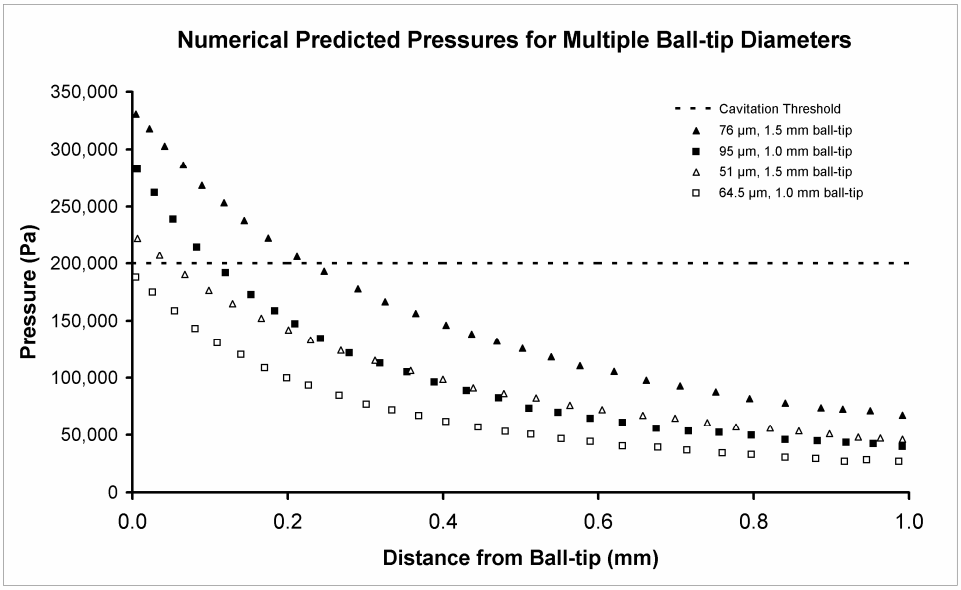

Figure 13: Predicted pressure field ahead of wire waveguide (distance 0 -1.0 mm) with 1.0 mm and 1.5 mm spherical ball-tips and multiple distal -tip displacements.

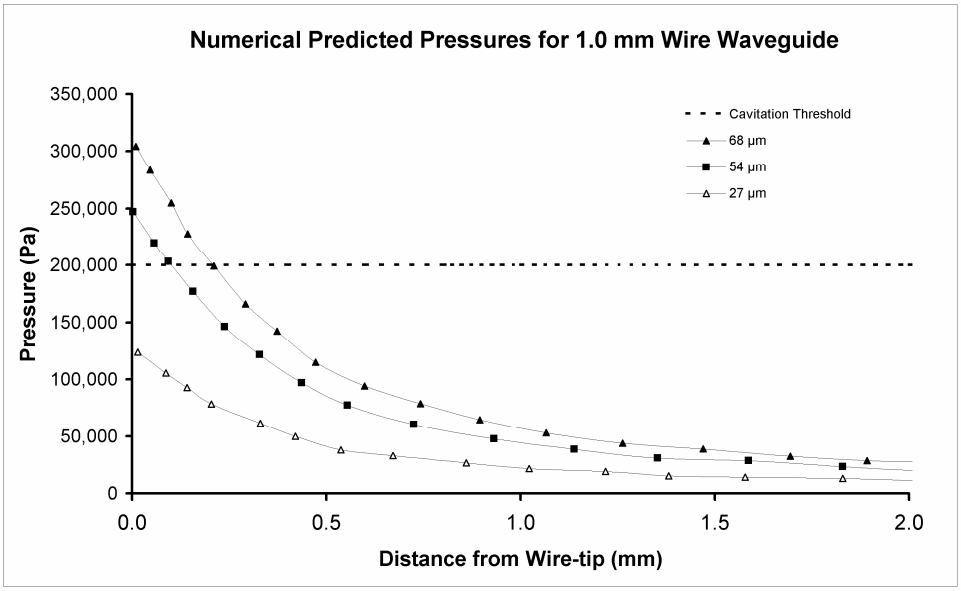

Figure 14: Predicted pressure field ahead of 1.0 mm diameter wire waveguide with a flat distal-tip and distal-tip displacements of 27, 54 and 68 µm.

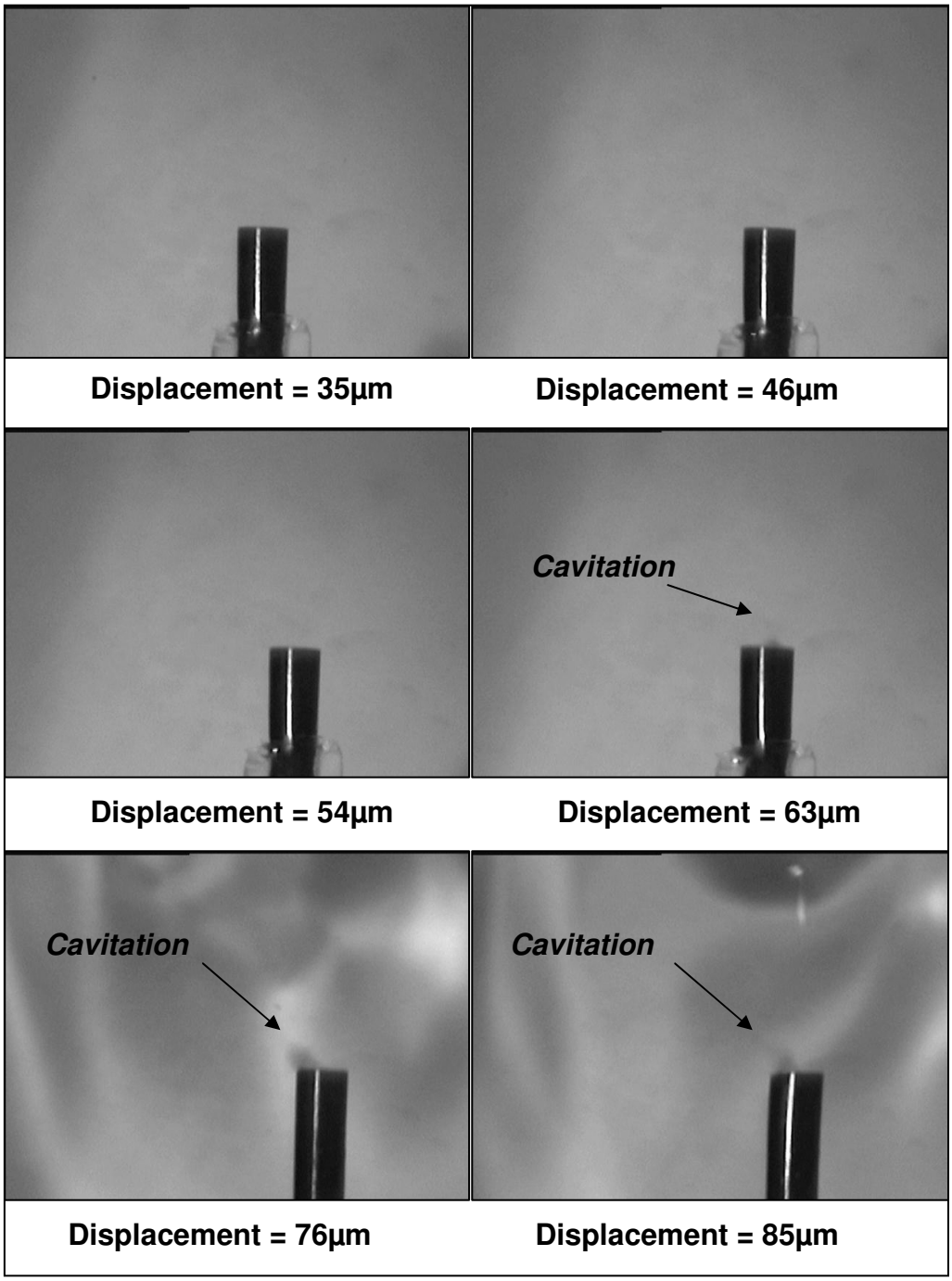

Figure 15: Images of the distal-tip of a 1.0 mm diameter wire waveguide vibrating at 23.5 kHz and with distal-tip displacements of 35, 46, 54, 63, 76 and 85 µm.

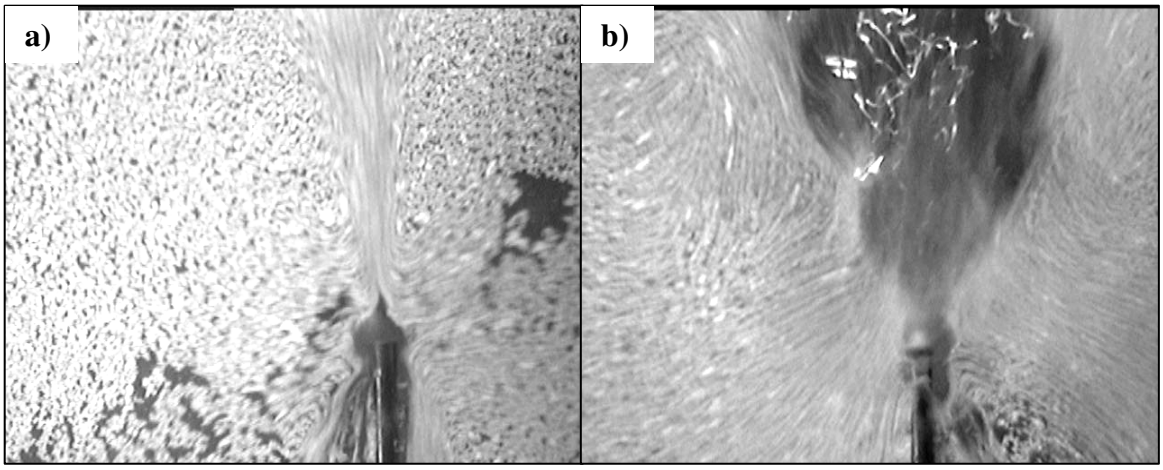

Figure 16: Image of fluid motion (acoustic streaming) around the distal-tip of a 1.0 mm diameter wire waveguide vibrating at 23.5 kHz and with distal-tip displacements of a) below predicted cavitation threshold = 35 µm and b) above predicted cavitation threshold = 76 µm.

Tables

Table 1: Material Properties

	Young's Modulus, E (GPa)	**Density, ρ** (kg/m^3)	**Speed of Sound, c** (m/s)
NiTi (56%Ni:Bal%Ti)	75	6450	3409
Blood	-	1580	1050